Journal of Marine Systems 76 (2009) 468–478

Contents lists available at ScienceDirect

Journal of Marine Systems

journal homepage: www.elsevier.com/locate/jmarsys

Air pollution history elucidated from anthropogenic spherules and their magnetic signatures in marine sediments offshore of Southwestern Taiwan

Chorng-Shern Horng [a,*], Chih-An Huh [a], Kuo-Hang Chen [a], Pin-Ru Huang [a], Kan-Hsi Hsiung [a], Hui-Ling Lin [b]

[a] Institute of Earth Sciences, Academia Sinica, P. O. Box 1-55, Nankang, Taipei, Taiwan 115-29, ROC
[b] Institute of Marine Geology and Chemistry, National Sun Yat-sen University, Kaohsiung, Taiwan 804-24, ROC

ARTICLE INFO

Article history:
Received 8 March 2007
Received in revised form 11 September 2007
Accepted 20 September 2007
Available online 26 August 2008

Keywords:
Air pollution
Magnetic spherules
Magnetic minerals
^{210}Pb dating

ABSTRACT

Kaohsiung City and its neighborhood in the southwestern coastal plain of Taiwan have suffered serious air pollution since the region became the largest center for heavy-industry on the island. In order to unravel the air pollution history of the region, four ^{210}Pb- and ^{137}Cs-dated sediment box cores recovered in 2006 from offshore of this area were chosen for magnetic and petrographic analyses. The data were used to distinguish changes in concentration, composition and grain size of magnetic particles in the sediments due to inputs of anthropogenic magnetic spherules. Sedimentation rates have been reasonably constant for the last one hundred years, except at the core tops which were affected by a turbidite layer induced by a typhoon in 2005. Down-core profiles of mass-specific magnetic susceptibility (χ) and saturation isothermal remanent magnetization (SIRM) are similar among the cores, and reflect similar trends to magnetic spherule counts. This reveals that χ and SIRM of modern marine sediments can be used as air pollution indicators for nearby industrialized upwind areas. The studied record indicates that industrialization of the area was gradual during 1950–1980 and boomed afterward, resulting in a high production of airborne magnetic spherules, which is consistent with evidence for poor air quality at that time. Optical and scanning electron microscopic (SEM) surveys of magnetic extracts indicate that the magnetic spherules have grain sizes ranging from a few micrometers up to 50 μm and consist mainly of iron oxides with variable Si, Al, and Ca contents. X-ray diffraction analysis on magnetic extracts from different depths in the cores further indicates that magnetite and pyrrhotite, which are derived from terrigenous detritus, form the magnetic constituents of the sediments before the area was industrialized. In contrast, during the industrial boom, anthropogenic magnetite and hematite spherules became the dominant magnetic particles in the sediments. Down-core profiles of hard isothermal remanent magnetization (HIRM) below the turbidite layer also reveal similar trends to the corresponding magnetic spherule counts, which indicate that the concentration of hematite in the sediments is also closely related to the extent of air pollution. In addition, relatively low values of χ_{ARM}/χ, which are indicative of coarse magnetic grains, started to occur when large magnetite spherules became significant during the industrialized period. The air pollution history elucidated from our sediment core data not only reflects the development of Kaohsiung from a small village to a highly industrialized metropolitan area in the 20th century, but it is also consistent with the most recent air pollution trends revealed by real time air quality measurements of PM_{10}. Our results demonstrate the usefulness of magnetic parameters for delineating the air pollution history of coastal marine sediments down-wind of nearby industrialized regions.

1. Introduction

Magnetic particles in continental margin marine sediments are usually derived primarily from terrestrial sources

* Corresponding author. Tel.: +886 2 2783 9910; fax: +886 2 2783 9871.
E-mail address: cshorng@earth.sinica.edu.tw (C.-S. Horng).

0924-7963/$ – see front matter © 2008 Elsevier B.V. All rights reserved.
doi:10.1016/j.jmarsys.2007.09.014

via fluvial and eolian transportation. Since industrialization, however, magnetic spherules originating from anthropogenic fly-ashes from factories and vehicles may also significantly contribute to the magnetic properties of marine sediments. This is especially common in coastal settings and marginal seas adjacent to heavily populated and industrialized areas. Although magnetic methods have been widely used to monitor air pollution (Thompson and Oldfield, 1986; Maher and Thompson, 1999; Evans and Heller, 2003), they have been mainly applied to urban dusts, soils, fluvial, lacustrine and estuarine sediments (Versteeg et al., 1995; Georgeaud et al., 1997; Heller et al., 1998; Chan et al., 1998; Petrovský et al., 2000; Jordanova et al., 2004; Spassov et al., 2004; Chaparro et al., 2006). Thus far, anthropogenic magnetic spherules in marine sediments have been reported in several studies (e.g., Doyle et al., 1976; Scoullos et al., 1979; Hunt, 1986), but little attention has been paid to construct long-term air pollution records based on such spherules. Compared with most environmental archives, coastal sediments may provide more favorable conditions for the preservation of historical air pollution records. This is because marine sedimentation is usually a reasonably continuous and steady process, and sediment layers can be dated by fallout radionuclides such as ^{210}Pb and ^{137}Cs to establish a reliable sediment chronology.

Taiwan's largest industrial city, Kaohsiung, is located on the coastal plain of southwestern Taiwan (Fig. 1). In the city and its neighborhood, many heavy-industry plants were established after the Second World War (1945 AD). Abundant magnetic spherules have been found in marine surficial sediments offshore of Kaohsiung (Horng and Roberts, 2006). The spherules coexist with detrital magnetic minerals transported from the drainage basin of the Gaoping (Kaoping) River (Fig. 1). Due to the high sediment load of this river (49 Mt/yr; Dadson et al., 2003) and resultant high sedimentation rates

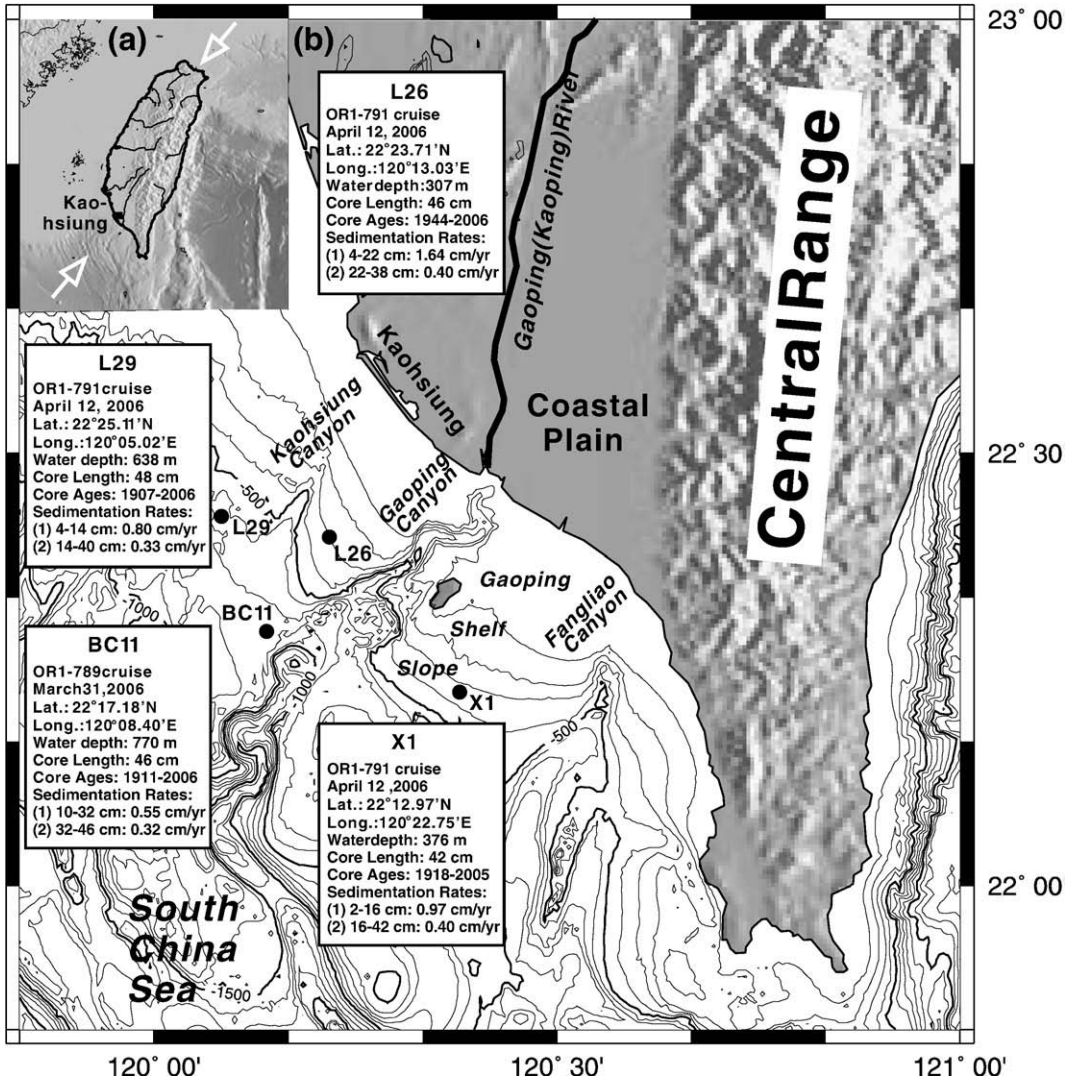

Fig. 1. (a) Map of Taiwan. The square indicates the location of the largest heavy-industry city, Kaohsiung, in Taiwan. The arrows indicate the southwesterly and northeasterly monsoons that prevail in southern Taiwan during the summer and winter, respectively. (b) A bathymetric and topographic map with locations and information for the box cores (L29, L26, BC11 and X1) recovered offshore of Kaohsiung City.

offshore of southwestern Taiwan (2mm/yr on average; Huh et al., 2009-this issue), it is possible to construct a detailed sediment chronology for magnetic spherule deposition using ^{210}Pb and ^{137}Cs dating. The purpose of this study is to decipher the historical air pollution record of the Kaohsiung area by integrating the sediment chronology with a magnetic study on the sediments.

We selected four relatively well dated sediment cores for this study. Magnetic properties of the sediments were analyzed for concentration, composition, and grain size of magnetic minerals to identify magnetic signatures associated with anthropogenic magnetic spherules. Petrographic methods including magnetic spherule counting, X-ray diffraction analysis (XRD), and scanning electron microscopic (SEM) observations were also employed using magnetic extracts from the sediments to facilitate data interpretation and corroboration.

2. Materials and methods

The four cores used for this study (BC11, L26, L29 and X1) were recovered in March and April, 2006, along with another 51 box cores during two cruises onboard R/V Ocean Researcher-1 (OR1-789 for BC11 and OR1-791 for L26, L29 and X1). They were located in a depositional lobe at water depths of 300–770 cm on the Gaoping slope (Fig. 1). These four cores were chosen because they provide better time resolution (1–8 years for 2-cm intervals; Huh et al., 2009-this issue) than other cores and their lengths are long enough (42–48 cm) to cover about one hundred years of history. It should be noted that a turbidite layer occurs at the tops of these cores (i.e., 0–4 cm for L26 and L29, 0–2 cm for X1, and 0–10 cm for BC11), which has been deciphered as an event layer induced by Typhoon Haitang during July 18–20, 2005 (Huh et al., 2009-this issue). Barring this layer, the cores have fairly steady sedimentation rates throughout their lengths. Detailed core information is presented in Fig. 1.

Sediment cores that had already been sampled at 2-cm intervals, freeze-dried and non-destructively analyzed for radionuclides were subsequently sampled with ~ 7-cm^3 plastic cubes for this study. In order to express magnetic parameters in mass-specific terms, ~ 8 g of sediment was weighed with a precision of 0.1mg for each specimen. The low-field magnetic susceptibility (χ) of all specimens was measured with a Bartington Instruments MS2B magnetic susceptibility meter. Using a 2G Enterprises triaxial degausser, anhysteretic remanent magnetizations (ARMs) were imparted along the *z*-axis of the specimens in a 0.05 mT direct current (DC) bias field with a maximum peak alternating field of 90 mT. ARMs were then measured with a 2G Enterprises superconducting rock magnetometer and values of χ_{ARM}, termed ARM susceptibility, were obtained by dividing ARM with the DC bias field. Subsequently, saturation isothermal remanent magnetizations (SIRMs) were imparted along the specimen *z*-axis using a DC field of 0.95 T generated using a 2G Enterprises pulse magnetizer. SIRM measurements were made with the 2G Enterprises rock magnetometer. To determine the S-ratio and hard isothermal remanent magnetization (HIRM), a reversed DC field of 0.3 T was applied to the specimens after measuring the SIRMs. Measurements of this magnetization, denoted as $IRM_{-0.3T}$, were made using the rock magnetometer. S-ratios and HIRMs were calculated following the definitions of King and Channell (1991) [i.e., S-ratio = − $IRM_{-0.3T}$/SIRM, and HIRM = ($IRM_{-0.3T}$ + SIRM) / 2].

In order to interpret the magnetic measurements and to identify the dominant magnetic minerals in the sediment samples, magnetic extractions were made using extra freeze-dried samples for three cores (L29, BC11 and X1). Representative fractions were obtained by subdividing bulk sediment samples with a splitter; 500 mg of the splits were weighed with a precision of 0.01 mg in a temperature- and humidity-controlled room. After making a slurry by adding water to the 500-mg samples, magnetic extraction was performed using a rare-earth magnet housed in a glass sheath. Standardized procedures were strictly followed by running the magnetic extraction five times, three minutes each time, to ensure that the amounts of magnetic spherules in the magnetic extracts can be compared without bias for samples obtained from each core. The magnetic extracts were cleaned in an ultrasonic bath and were then demagnetized at 100 mT peak alternating field to help minimize particle clumping. Subsequently, Whatman 10-μm and 2-μm membrane filters (25 mm diameter) were used to collect magnetic grains with sizes larger than 10 μm and between 10 and 2 μm from each magnetic extract. The number of magnetic spherules retained on the 10-μm filters was counted under a Zeiss reflective light microscope by examining 25 microscopic fields of view (× 200 magnification) in each run. For samples that contain small spherule concentrations (<30 for each run), two to three runs were made so as to improve the counting statistics, and the results were averaged. Counting was focused on magnetic spherules larger than 10 μm and was confined to 25–75 fields of view under the microscope, therefore this method can be only regarded as semi-quantitative (or comparative) rather than absolute.

Following microscopic examination and magnetic spherule counting, observations of magnetic extracts were made using a JOEL JSM-6360LV SEM operated at 15 Kev with 18 nA acceleration voltage. Chemical spectra of minerals were obtained using an Oxford Instruments Ltd. INCA-300 X-ray energy dispersive spectrometer (EDS). XRD analysis was also carried out on selected magnetic extracts using a Rikagu Miniflex table top unit (Cu-α radiation). The X-ray scans were run from 4° to 80° (2θ). Results are presented after subtraction of the background trend.

3. Results and discussion

3.1. Anthropogenic spherules as the major contributor of magnetic particles to the sediments

The χ signal is mainly derived from ferrimagnetic substances; therefore this parameter has been widely used to estimate magnetic mineral concentrations in sediment samples. The measured χ values are plotted versus down-core depth along with ^{210}Pb- and ^{137}Cs-derived chronologies to compare temporal variations of χ in the studied cores (Fig. 2a). It is clear from Fig. 2a that the cores have relatively low and invariable χ before *ca.* 1950. Afterwards, the χ values first increased gradually but then drastically prior to reaching the maximum at around 1990–1994. Above this maximum value, χ decreases upward toward the present. Finally, at the core tops where a typhoon-induced turbidite layer was deposited, χ values are lowest, particularly for cores L26, BC11 and X1.

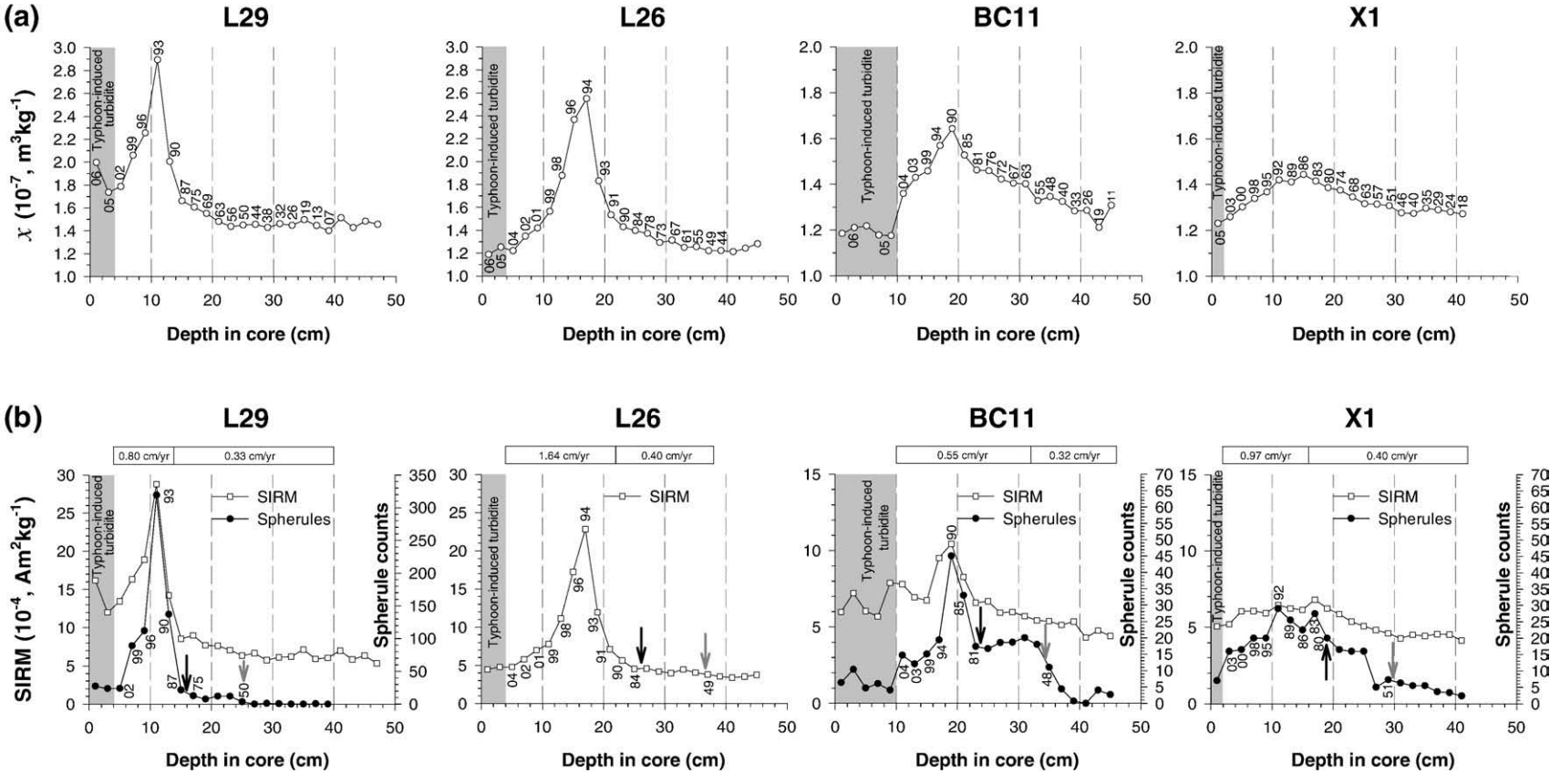

Fig. 2. (a) Down-core profiles of mass-specific magnetic susceptibility (χ) in box cores L29, L26, BC11 and X1. Ages of the sediment horizons are indicated along the profiles (06 represents 2006, 63 indicates 1963, etc.), which are based on ^{210}Pb- and ^{137}Cs-derived chronologies (Huh et al., 2009-this issue). The gray shaded intervals are turbidite deposits induced by Typhoon Haitang during July 18–20, 2005. (b) Down-core profiles of mass-specific SIRM (open squares) in the studied cores (left y-axis). The numbers of magnetic spherules (solid dots) counted from magnetic extracts of L29, BC11 and X1 are also plotted (right *y*-axis). Ages for some horizons are indicated along the profiles. Dark-gray and black arrows indicate 1950 AD and 1980 AD, respectively. Sedimentation rates derived from each core are shown in horizontal bars at the top.

SIRM variations are shown in Fig. 2b for the four cores. Values of SIRM are related to the concentration of magnetic minerals that carry remanent magnetizations. The measured SIRM profiles have similar trends to χ in each core, although they are not consistent at some horizons, such as at 1999 AD and 2003 AD in core BC11. In each core, the SIRM trend follows the magnetic spherule counts (Fig. 2b), indicating that anthropogenic spherules are the major magnetic contributor to the SIRM signature of the modern sediments. By comparing the magnetic spherule counts among cores L29, BC11, and X1, it is clear that the counts decrease offshore away from Kaohsiung (Figs. 1b and 2b). We therefore conclude that the magnetic spherules were transported by wind from the Kaohsiung area and that they are related to air pollution in the region. When assigning ages to the magnetic spherule counts in each core and comparing trends in the SIRM and χ profiles (Fig. 2a–b), it is clear that all four cores have similar profiles. SIRM and χ of these modern continental margin sediments can therefore be used as historical air pollution indicators for the nearby industrialized area. Our record indicates that, before *ca.* 1950, the Kaohsiung area was in the pre-industrialization stage. During the 1950–1980 interval, industrialization started to develop. Afterwards, the industrial boom resulted in poor regional air quality. It should also be noted that as a result of increased human activities in the Gaoping River catchment, sedimentation rates in the offshore area, such as at sites L29, L26 and X1, have increased dramatically since the end of the 1980s (Figs. 1b and 2b). Although the increase in sediment flux would dilute the concentration and thus result in lower counts of magnetic spherules, our estimation of the depositional flux of any wind-blown pollutant particles has not been biased by this effect.

3.2. Composition of magnetic minerals from different transport pathways

Optical and SEM images of magnetic spherules shown in Fig. 3a and b indicate that the grain sizes of the spherules range from a few micrometers up to 50μm. The spherules can be divided into three groups based on their color and luster, as observed under the optical microscope (Fig. 3a). Spherules of the first group are black and have a shining metallic luster (Fig. 3a-1). In contrast, those of the second group are lackluster and lighter (Fig. 3a-2). The third group of spherules has intermediate color with rusty tints (Fig. 3a-3). These differences in spherule color, brightness and luster reflect different mineralogical compositions. SEM observations with EDS chemical analysis on the spherules reveal that the brighter spherules are Fe-oxides and that the darker ones consist of Fe-oxides with variable contents of Si, Al, and Ca (Fig. 3b-c). Although we did not quantify the ratio between ferric (Fe^{3+}) and ferrous (Fe^{2+}) iron for the spherules using SEM/EDS, the rusty spherules (i.e., the third type observed under the optical microscope) must contain more Fe^{3+} than the other two types of spherules. Surface textures typical of these spherules are illustrated in Fig. 3d-f.

XRD analysis on magnetic extracts further characterizes the dominant magnetic minerals in sediment horizons representing the periods of pre-industrialization (prior to 1950), severe air pollution (1990–1999) and the recent flood deposit caused by Typhoon Haitang (2005 AD) (Fig. 4). In the pre-industrial period, magnetite is the dominant magnetic mineral, which coexists with small amounts of pyrrhotite (Fig. 4a), both of which are known to occur as terrigenous detritus in the Gaoping catchment (Horng and Roberts, 2006). During the period of severe air pollution, magnetite and hematite occur as magnetic spherules and are the major magnetic particles, which enhance XRD counts derived from detrital magnetite and pyrrhotite in the terrigenous substrate (Fig. 4b). Based on the XRD results, we conclude that the first and the third types of magnetic spherules identified based on optical microscopic classification are composed of magnetite and hematite, respectively. Pyrrhotite replaces magnetite to become the dominant magnetic mineral in the typhoon-induced turbidite layer (Fig. 4c), which indicates substantial headwater erosion and input of sediments transported from pyrrhotite-bearing metamorphic terrains in the Central Range (Fig. 1b) (Horng and Roberts, 2006).

3.3. Contributions of different magnetic minerals to the sediment sequences

In view of the difference in coercivity between magnetite, pyrrhotite and hematite in most natural and synthetic samples (Horng et al., 1992; Roberts et al., 1995, 2006), the S-ratio and HIRM, which are both coercivity-dependent parameters, can be employed to assess relative contributions of these magnetic minerals to the sediments in different time periods. Profiles of the S-ratio and HIRM in the studied cores are shown in Fig. 5. It is clear from Fig. 5a that the S-ratio falls within the 0.92–0.96 range at all depths except in the surface turbidite layer and in the 1919 AD horizon in core BC11. The high (close to 1) S-ratio indicates that magnetite, either of natural or anthropogenic origin, is the major magnetic mineral before and after industrialization of the Kaohsiung area. However, the HIRM curves, which are similar to the corresponding trends of magnetic spherule counts (Fig. 5b), further reveal that the contribution of anthropogenic hematite spherules cannot be neglected after industrialization of the region, particularly during the period with the most intense air pollution. It should be also noted that in the typhoon-induced turbidite layer, the dominance of pyrrhotite, which has high coercivity relative to magnetite, has resulted in a decrease in the S-ratio and an increase in HIRM (Fig. 5). Based on this observation, we infer that the abnormal values of S-ratio and HIRM found in pre-industrialization horizons, such as the 1919 AD and 1955 AD horizons in core BC11 (Fig. 5), could be due to emplacement of pyrrhotite-enriched storm event layers.

From a comparison between Fig. 5a and b, we observe that HIRM is a more sensitive parameter than the S-ratio for indicating the contribution of anthropogenically produced high-coercivity magnetic particles (e.g., hematite) to the sediments. For instance, concentrations of anthropogenic hematite should be higher in sediment layers deposited during the period of severe air pollution (1990–1999), as indicated by the relatively high values of HIRM (Fig. 5b). However, the S-ratios in the studied cores, except for core L29, do not have lower values corresponding to higher HIRMs. At the other three sites, particularly L26, sediment accumulation is more affected by fluvial transport from the Gaoping River (Fig. 1b). Magnetite, not only from artificial but also from natural sources, is therefore constantly the dominant magnetic mineral even during the period of high air pollution. Thus, increased hematite concentrations in the other three cores will not significantly decrease the S-ratio.

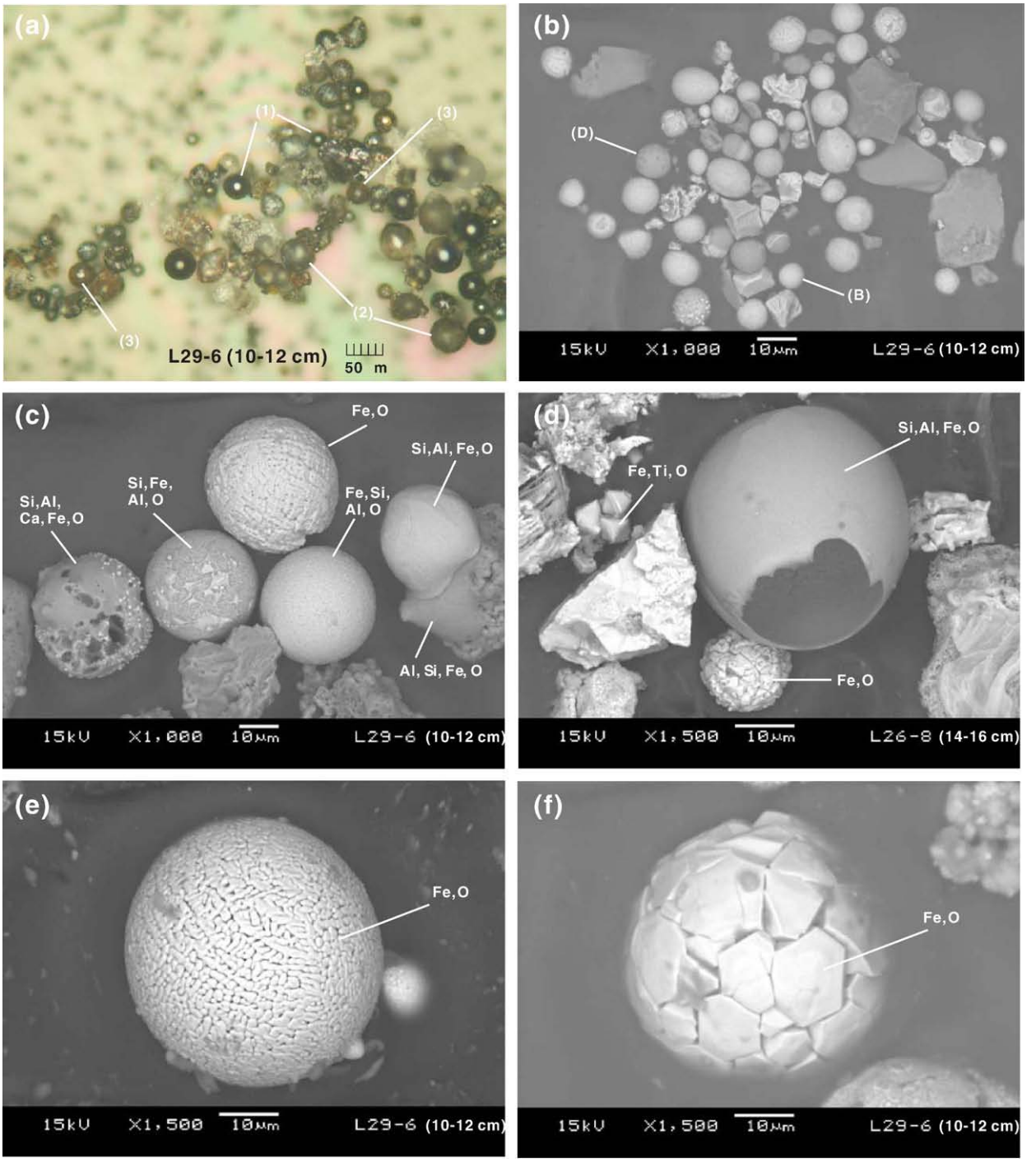

Fig. 3. (a) Photograph of magnetic spherules under optical microscope revealing various grain sizes up to 50 μm and displaying three types of color and luster (see text for explanations). Underneath the spherules is a 10-μm filter. (b–f) Back-scattered electron microscopic images of magnetic spherules: (b) bright (B) and dark (D) spherules with grain sizes smaller than 10 μm. (c) Major chemical elements of spherules showing different shades and surface textures. (d) The larger, broken hollow spherule with a smooth surface is an iron oxide containing Si and Al. Two smaller iron minerals shown on the picture are probably magnetite and titanomagnetite, respectively. (e) and (f) iron-oxide spherules with brain-like and framboid-like surface textures, respectively.

3.4. Variations in magnetite grain size from different sources

Magnetite is common throughout the length of the studied cores; therefore we used the χ_{ARM}/χ ratio as a measure of relative size variation of magnetite grains in the sediment cores (Banerjee et al., 1981; King et al., 1982). Down-core profiles of χ_{ARM}/χ are shown in Fig. 6. These profiles have the lowest χ_{ARM}/χ values at the core tops, suggesting that the typhoon-induced turbidite layer contains relatively coarse-grained magnetite. This result is reasonable because a turbidite event usually

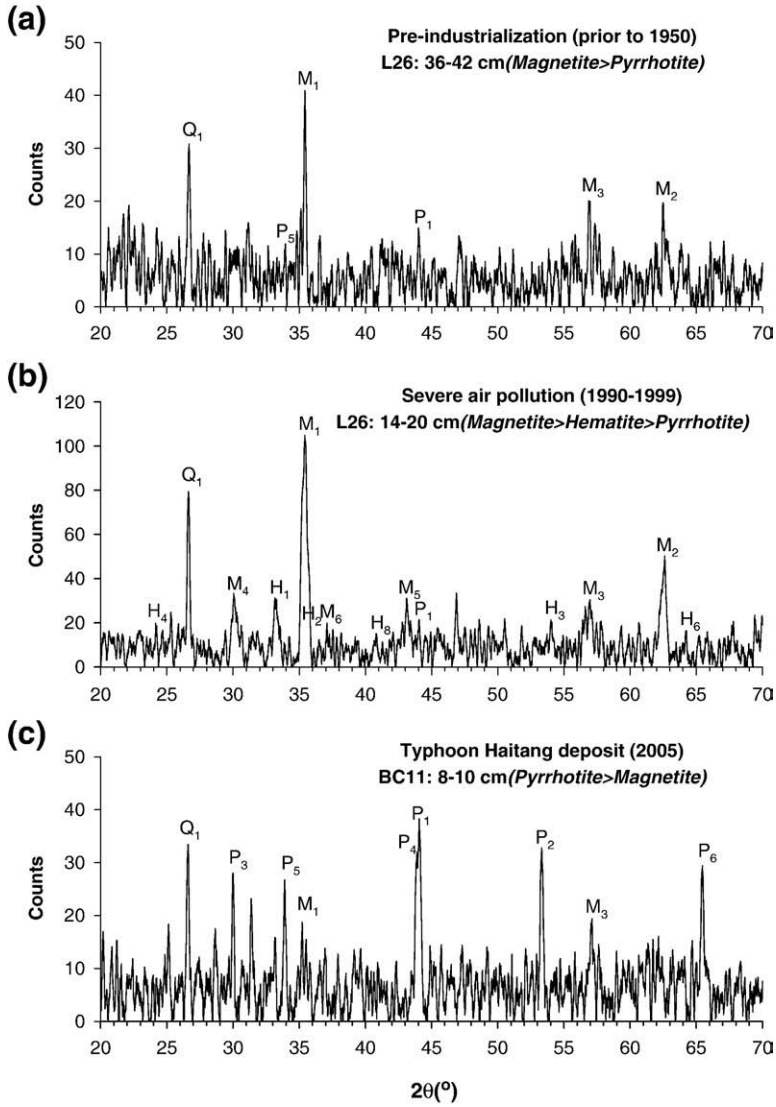

Fig. 4. X-ray diffractograms of magnetic extracts from three sediment horizons covering the (a) pre-industrialization period (prior to 1950), (b) severe air pollution period (1990–1999), and (c) the recent flood layer caused by Typhoon Haitang (2005 AD). The main peaks for magnetite (M_1–M_6), hematite (H_1–H_8), monoclinic pyrrhotite (P_1–P_6), and quartz (Q_1) are marked. The dominance of magnetic minerals is based on their peak intensities (counts). Some peaks cannot be identified due to low magnetic mineral concentrations.

results in poorly-sorted and coarser-grained sediment deposition than surrounding sediments. By extension, the abrupt χ_{ARM}/χ minima at depth (the hatched bars in Fig. 6) can probably be attributed to turbidites deposited prior to industrialization of the region. There are fairly good time correlations among the turbidite layers delineated in cores L29, BC11 and X1.

We also observe from Fig. 6 that before industrialization of the Kaohsiung area, the χ_{ARM}/χ ratios increase gradually after the proposed turbidite events, implying that the grain sizes of detrital magnetite decrease upwards. However, after the area was industrialized, the offshore sedimentary environment started to receive an additional input of coarser-grained magnetite from anthropogenic spherules, and the fining-upward trend of the χ_{ARM}/χ curves is disrupted, depending on the grain sizes and abundances of anthropogenic spherules. For instance, during 1950–1980, the anthropogenic spherule concentrations were low and these coarser particles were mainly transported to the near-shore sites, namely L29 and L26, causing a decrease of χ_{ARM}/χ after the 1960s (Fig. 6). However, it was not until circa 1985 that the input of coarser spherules was sufficient to decrease the χ_{ARM}/χ ratio in cores BC11 and X1, which suggests a time lag for the distal sites to record the domination of larger magnetite grains associated with air pollution. Since about 1990, the dominant contribution of coarse magnetite spherules to the marine sediments caused by high air pollution has resulted in low values of χ_{ARM}/χ at all four sites.

3.5. Comparison between the sedimentary record of air pollution and real time air quality data

Since July 1993, the Environmental Protection Administration of Taiwan has continuously monitored the air quality

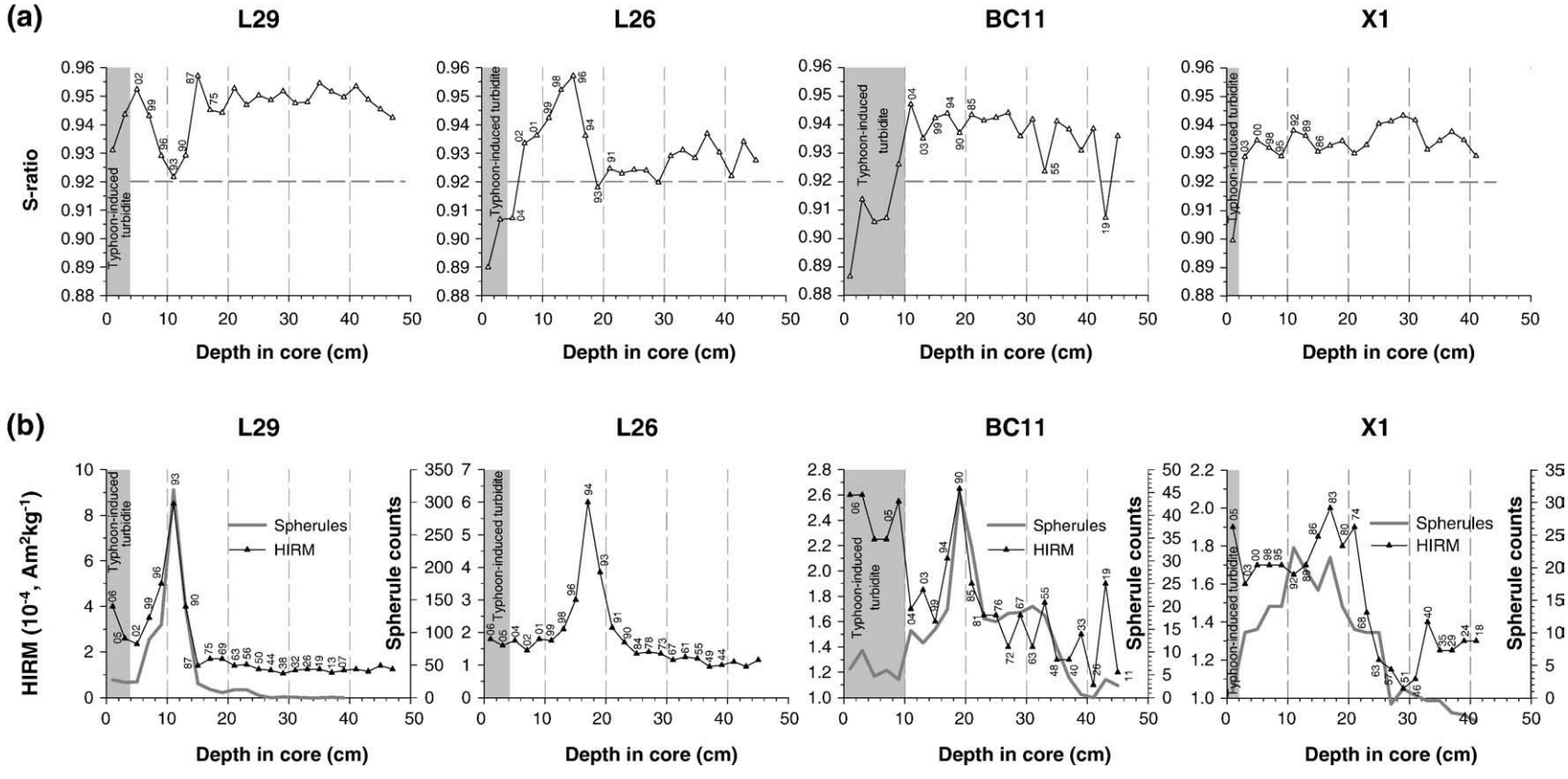

Fig. 5. (a) Down-core profiles of the S-ratio in box cores L29, L26, BC11 and X1. Horizontal dashed lines indicate an S-ratio of 0.92. (b) Comparison of down-core profiles of HIRM (solid triangles) and magnetic spherule counts (dark gray lines) in the studied cores. The scales for spherule counts in cores BC11 and X1 have been exaggerated (×1.4 and ×2.0, respectively) relative to the corresponding plots in Fig. 2b.

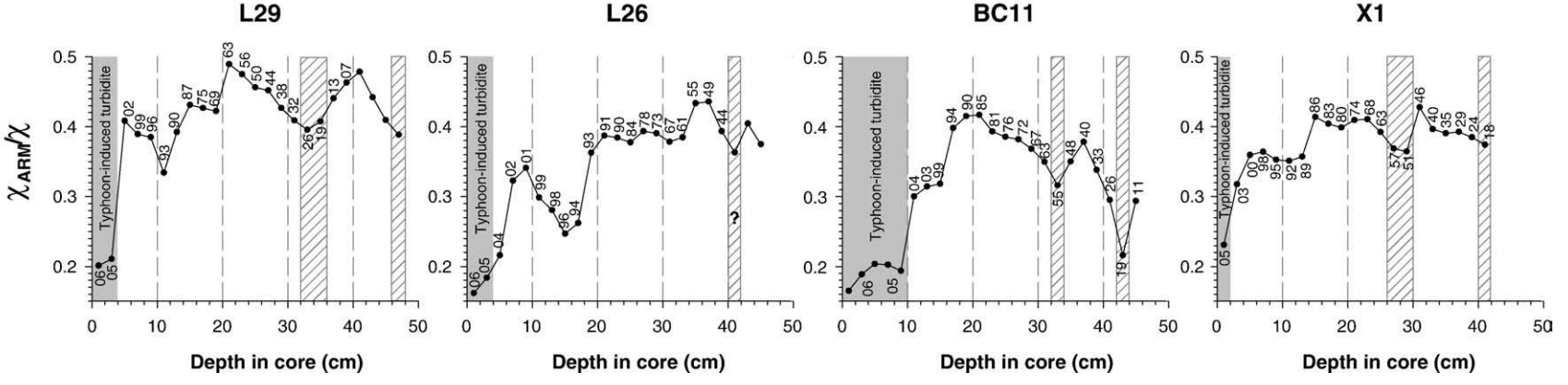

Fig. 6. Down-core profiles of χ_{ARM}/χ in box cores L29, L26, BC11 and X1, which indicate variations in magnetite grain size. Some possible turbidite layers that occurred prior to industrialization are marked with hatched bars. These layers probably represent deposition associated with storm events.

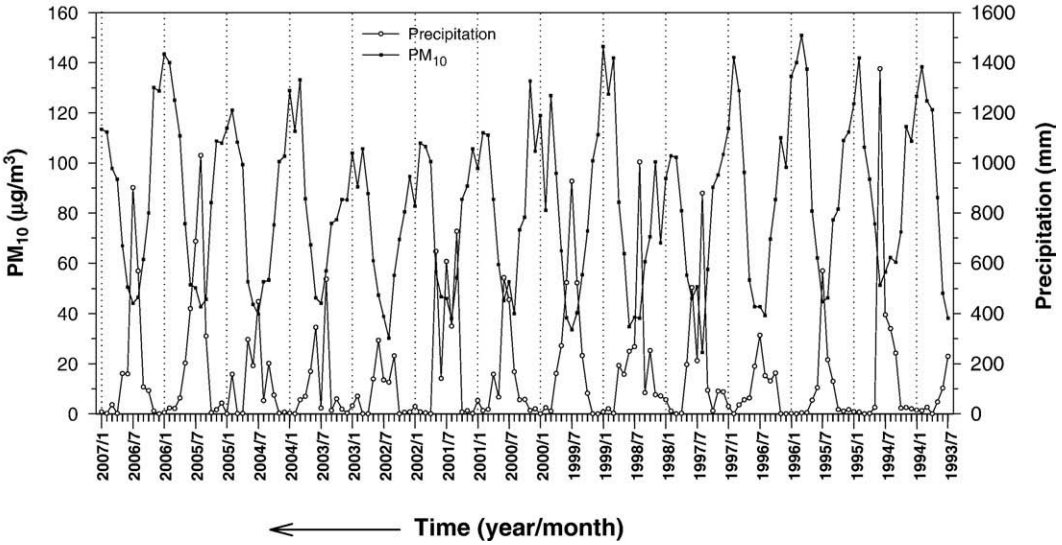

Fig. 7. Real time monthly means of PM_{10} and precipitation for Kaohsiung City from July, 1993 to January, 2007. The PM_{10} data are from the industry monitor station (Cianjhen) in Kaohsiung operated by the Environmental Protection Administration (EPA) of Taiwan, and the precipitation data are from the Kaohsiung station of the Central Weather Bureau (CWB) of Taiwan. The data are available from the EPA and CWB websites (http://210.69.101.141/emce/ and http://cwb.gov.tw/V5e/, respectively).

of the Kaohsiung area. Suspended particulate matter in air with grain sizes less than 10 μm (PM_{10}) was collected with an automatic filter sampler and its concentration (μg/m^3) was measured hourly using the beta-ray absorption technique. The time-series data of PM_{10} (Fig. 7) clearly reveal the most recent history of industrialization and population growth in the area.

According to official demographic data, the population of Kaohsiung has increased from ~ 3000 in 1900 to more than 1.5 million at present. This 500-fold population increase reflects the development of a rural area into a highly industrialized metropolitan area. During the pre-industrial stage of 1900–1950, the population of the area grew by a factor of almost 90, mainly due to a mass exodus from mainland China in the wake of a civil war after the Second World War. Since then, Kaohsiung City and its satellite towns have been transformed into the heavy-industry hub of Taiwan, with increased establishment of oil refineries (in 1946 and 1976) and factories for the production of cement (in 1954 and 1958), electricity (in 1967 and 1977), and steel (in 1982). Along with the industrialization and economic boom, increased population growth occurred at mean rates of 20,000/yr during 1950–1960 and 37,000/yr during 1960–1980. Since 1980, the population growth rate has gradually slowed, from 18,000/yr during 1980–1990 to 8,000/yr afterwards. At present, the city's population density (9860/km^2) is the highest in Taiwan.

The pollution time series in Fig. 7 clearly shows high PM_{10} (hence poor air quality) each year from October to March of the next year. This is tied to the annual cycle of monsoons and rainfall in southern Taiwan. Air quality is poor primarily in the winter when dry and cold northeasterly winds from the Asian continent prevail over the area (Fig. 1a). In contrast, wet and warm southwesterly winds from the South China Sea prevail in the summer, which is also the typhoon season. Conceivably, suspended particulates can be more easily removed from the air in the summer by wet precipitation, but they remain airborne longer during the dry winter and are blown to sea by northeasterly winds.

PM_{10} values were high during the winters of 1993–1999, except in 1997. Lower PM_{10} in the winter of 1997 may be related to abnormally higher precipitation associated with the 1997/98 El Niño. The data suggest that air quality improved from 1999 to 2002 (for details see http://www.epa.gov.tw/en/index.aspx), but deteriorated again in the last three years. Our sediment core data also suggest high air pollution during 1993–1999 and an improvement during 1999–2003 (Fig. 2b). Unfortunately, the most recent record (i.e., during 2003–2006) is blurred by emplacement of the turbidite layer in 2005. In summary, although air quality data are not available prior to 1993, the correspondence between the sedimentary record near the tops of the studied cores and the real time air quality data since 1993 points to the value of sediment cores as archives of longer, otherwise undocumented pollution history.

4. Conclusions

We have demonstrated that continental margin marine sediment cores containing magnetic spherules of anthropogenic origin may be used to decipher the history of air pollution for a nearby industrialized area. Along with development of the industrialized area, more anthropogenic magnetic spherules in the polluted air were transported to sea via prevailing winds, which caused significant changes in magnetic properties of the sediments. Magnetic methods helped to rapidly identify changes in magnetic mineral-concentration, composition and grain size in the marine sediments, and to successfully discriminate the contribution of anthropogenic magnetic spherules from natural, detrital magnetic particles. This is the first such study in the Taiwan area. To further substantiate this method and to apply it to environmental and pollution studies, more detailed sampling for better time resolution is needed for future work.

Regardless, this approach should be useful for understanding the pollution history of industrialized areas, and the background levels that should be aimed for, if realistic reduction of pollution can be achieved.

Acknowledgements

We are grateful to Yoshi Iizuka for technical assistance in SEM analysis and to James T. Liu for encouraging us to use the marine cores of the FATES-KP research program for this study. Andrew Roberts and an anonymous reviewer made comments that improved this paper. This work is supported by the Institute of Earth Sciences, Academia Sinica and by National Science Council Grants NSC94-2611-M-001-003 and 95-2611-M-001-002.

References

Banerjee, S.K., King, J.W., Marvin, J., 1981. A rapid method for magnetic granulometry with applications to environmental studies. Geophys. Res. Lett. 8, 333–336.

Chan, L.S., Yeung, C.H., Yim, W.W.-S., Or, O.L., 1998. Correlation between magnetic susceptibility and distribution of heavy metals in contaminated sea-floor sediments of Hong Kong Harbour. Environ. Geol. 36, 77–86.

Chaparro, M.A.E., Gogorza, C.S.G., Chaparro, M.A.E., Irurzun, M.A., Sinito, A.M., 2006. Review of magnetism and heavy metal pollution studies of various environments in Argentina. Earth Planets Space 58, 1411–1422.

Dadson, S.J., Hovius, N., Chen, H., Dade, W.B., Hsieh, M.-L., Wilett, S.D., Hu, J.-C., Horng, M.-J., Chen, M.-C., Stark, C.P., Lague, D., Lin, J.-C., 2003. Links between erosion, runoff variability and seismicity in the Taiwan orogen. Nature 426, 648–651.

Doyle, J.L., Hopkins, T.L., Betzer, P.R., 1976. Black magnetic spherule fallout in the eastern Gulf of Mexico. Science 194, 1157–1159.

Evans, M.E., Heller, F., 2003. Environmental magnetism: principles and applications of enviromagnetics. Academic Press, San Diego.

Georgeaud, V.M., Rochette, P., Ambrosi, J.P., Vandamme, D., Williamson, D., 1997. Relationship between heavy metals and magnetic properties in a large polluted catchment: the Etang de Berre (south of France). Phys. Chem. Earth 22, 211–214.

Heller, F., Strzyszcz, Z., Magiera, T., 1998. Magnetic record of industrial pollution in forest soils of Upper Silesia, Poland. J. Geophys. Res. 103, 17767–17774.

Horng, C.-S., Laj, C., Lee, T.-Q., Chen, J.-C., 1992. Magnetic characteristics of sedimentary rocks from the Tsengwen-chi and Erhjen-chi sections in southwestern Taiwan. Terr. Atmos. Oceanic Sci. 3, 519–532.

Horng, C.-S., Roberts, A.P., 2006. Authigenic or detrital origin of pyrrhotite in sediments?: resolving a paleomagnetic conundrum. Earth Planet. Sci. Lett. 241, 750–762.

Huh, C.-A., Lin, H.-L., Lin, S., Huang, Y.-W., 2009. Modern accumulation rates and a budget of sediment off the Gaoping River, SW Taiwan: a tidal and flood dominated depositional environment around a submarine canyon. J. Mar. Sys. 76, 405–416 (this issue). doi:10.1016/j.jmarsys.2007.07.009.

Hunt, A., 1986. The application of mineral magnetic methods to atmospheric aerosol discrimination. Phys. Earth Planet. Int. 42, 10–21.

Jordanova, D., Hoffmann, V., Fehr, K.T., 2004. Mineral magnetic characterization of anthropogenic magnetic phases in the Danube River sediments (Bulgarian part). Earth Planet. Sci. Lett. 221, 71–89.

King, J., Banerjee, S.K., Marvin, J., Özdemir, Ö., 1982. A comparison of different magnetic methods for determining the relative grain size of magnetite in natural materials: some results from lake sediments. Earth Planet. Sci. Lett. 59, 404–419.

King, J.W., Channell, J.E.T., 1991. Sedimentary magnetism, environmental magnetism, and magnetostratigraphy. U.S. National Report to International Union of Geodesy and Geophysics 1987–1990. Rev. Geophys. 29, 358–370.

Maher, B.A., Thompson, R. (Eds.), 1999. Quaternary Climates, Environments and Magnetism. Cambridge University Press, Cambridge.

Petrovský, E., Kapicka, A., Jordanoa, N., Knob, M., Hoffmann, V., 2000. Low-field magnetic susceptibility: a proxy method of estimating increased pollution of different environmental systems. Environ. Geol. 39, 312–318.

Roberts, A.P., Cui, Y., Verosub, K.L., 1995. Wasp-waisted hysteresis loops: mineral magnetic characteristics and discrimination of components in mixed magnetic systems. J. Geophys. Res. 100, 17909–17924.

Roberts, A.P., Liu, Q., Rowan, C.J., Chang, L., Carvallo, C., Torrent, J., Horng, C-.S., 2006. Characterization of hematite (α-Fe_2O_3), goethite (α-FeOOH), greigite (Fe_3S_4), and pyrrhotite (Fe_7S_8) using first-order reversal curve diagrams. J. Geophys. Res. 111, B12S35. doi:10.1029/2006JB004715.

Scoullos, M., Oldfield, F., Thompson, R., 1979. Magnetic monitoring of marine particulate pollution in the Elefsis Gulf, Greece. Mar. Pollut. Bull. 10, 287–291.

Spassov, S., Egli, R., Heller, F., Nourgaliev, D.K., Hannam, J., 2004. Magnetic quantification of urban pollution sources in atmospheric particulate matter. Geophys. J. Int. 159, 555–564.

Thompson, R., Oldfield, F., 1986. Environmental Magnetism. Allen & Unwin, London.

Versteeg, J.K., Morris, W.A., Rukavina, N.A., 1995. Mapping contaminated sediment in Hamilton Harbour, Ontario. Geosci. Can. 22, 145–151.